Scaling and intermittent properties of oceanic and atmospheric $p\mathrm{CO_2}$ time series and their difference in a turbulence framework

Kévin Robache[1], François G. Schmitt[1], and Yongxiang Huang[2,3]

[1]Laboratoire d'Océanologie et Géosciences, Université du Littoral Côte d'Opale, Université de Lille, CNRS, IRD, UMR LOG 8187, 62930 Wimereux, France
[2]State Key Laboratory of Marine Environmental Science & Center for Marine Meteorology and Climate Change & College of Ocean and Earth Sciences, Xiamen University, Xiamen, China
[3]Fujian Engineering Research Center for Ocean Remote Sensing Big Data, Xiamen University, Xiamen, China

Correspondence: Kévin Robache (kevin.robache@univ-littoral.fr) and François G. Schmitt (francois.schmitt@cnrs.fr)

Abstract. In this study the multi-scale dynamics of 38 oceanic and atmospheric $p\mathrm{CO_2}$ time series from fixed Eulerian buoys recorded with three-hour resolution are considered and their multifractal properties are demonstrated. The difference between these time series, the sea surface temperature and the sea surface salinity data were also studied. These series possess multi-scale turbulent-like fluctuations and display scaling properties from three hours to the annual scale. Scaling exponents are estimated through Fourier analysis and their average quantities considered globally for all parameters, as well as for different ecosystems ~~(e.g. coastal shelf, coral reefs, open ocean)~~ such as coastal shelf, coral reefs and open ocean. Sea surface temperature is the only parameter for which a spectral slope close to $5/3$ is found, corresponding to a passive scalar in homogeneous and isotropic turbulence. The other parameters had smaller spectral slopes, from ~~1.18~~ 1.22 to ~~1.35~~ 1.45. By using empirical mode decomposition of the time series, together with generalized Hilbert spectral analysis, the intermittency of the time series was considered in the multifractal framework. Concave moment functions were estimated and Hurst index H and intermittency parameters μ estimated in the framework of a lognormal multifractal fit. We obtained mean values of $H = 0.26$ and 0.21 respectively for oceanic and atmospheric $p\mathrm{CO_2}$ time series and $\mu = 0.08$ for both. It is the first time that atmospheric and oceanic $p\mathrm{CO_2}$ and their difference $\Delta p\mathrm{CO_2}$ are studied using such intermittent turbulence framework. The $\Delta p\mathrm{CO_2}$ time series was shown to possess power-law scaling with an exponent of ~~$\beta = 1.32 \pm 0.2$~~ $\beta = 1.36 \pm 0.19$.

1 Introduction: turbulent ~~carbon dioxide~~ $\mathrm{CO_2}$ fluxes at the air-sea interface

Anthropogenic global carbon dioxide ($\mathrm{CO_2}$) emissions have been rising since the last century (Pathak et al., 2022; Liu et al., 2022), increasing from around 4.6 ± 0.7 GtC y^{-1} in the 1960s to around 11.1 ± 0.9 GtC y^{-1} in recent years (Friedlingstein et al., 2023), and are linked with climate change (Anderson et al., 2016; Alola and Kirikkaleli, 2021). These emissions are ~~mitigated~~ partially counterbalanced by different mechanisms at different scales, from climate to small scale turbulence. This is especially true in the oceans (Sabine et al., 2004), which absorbs around 25 % of annual anthropogenic emissions (Friedlingstein et al., 2023). It is known that several other mechanisms influence the $\mathrm{CO_2}$ dynamics in the ocean and the atmosphere at different spatial and temporal scales. For example, terrestrial biology (Keenan et al., 2012; Crisp et al., 2022), land chem-

istry (Roland et al., 2013), volcanism and human activities (Yue and Gao, 2018) can lead to variations of atmospheric CO_2.
Furthermore, the ocean plays a major role in the carbon cycle through its interactions with the atmosphere and can absorb or

25 release CO_2 via physical and biological pumps (De La Rocha and Passow, 2014; Yamamoto et al., 2018). These pumps are
composed of numerous oceanic processes which also enable carbon sequestration at different timescales in the water column,
e.g. through phytoplankton blooms and the thermo-haline circulation (Falkowski et al., 2000; De La Rocha and Passow, 2014)
and in the sediment (Henson et al., 2019).

Globally, at large temporal (e.g. annual) and spatial (e.g. planetary) scales, the ocean is a sink of ~~carbon dioxide~~ CO_2.

30 However, locally in time and space, the ocean may be a sink or a source of ~~carbon dioxide~~ CO_2. In order to understand this
better, ~~in-situ~~ *in situ* observations are necessary. Here we consider high-frequency fixed points data at different parts of the
global ocean, and focus on the influence of multiscale turbulence on their flux. The air-sea ~~carbon dioxide~~ CO_2 flux is usually
written as (Wanninkhof, 2014):

$$F_{CO_2} = k(U) \cdot K_0 \cdot \Delta \, pCO_2 \tag{1}$$

35 where K_0 is the solubility (mol L^{-1} atm^{-1}), $k(U)$ is the gas transfer velocity (cm h^{-1}) which depends on the surface wind speed
U, and $\Delta \, pCO_2 = pCO_2{}_{\text{sw}} - pCO_2{}_{\text{air}}$ is the difference between partial pressures of ~~carbon dioxide~~ CO_2 in equilibrium
with surface water and in the air above the seawater. Turbulence has a direct influence on the different components of this
formula: K_0 depends on temperature and salinity, which are turbulent scalars, k depends on wind turbulence on the atmospheric
surface, and $\Delta \, pCO_2$ depends on two scalars both advected by turbulence. Since k and K_0 are both positive parameters,

40 the direction of the flux is determined in the difference $\Delta \, pCO_2$: when $\Delta \, pCO_2 > 0$, the flux goes from the sea to the
atmosphere, and when $\Delta \, pCO_2 < 0$ the ocean is locally a sink of ~~carbon dioxide~~ CO_2. In this work we focus on the scaling
properties of atmospheric and oceanic ~~carbon dioxide~~ CO_2 partial pressures and on their difference, using a database of
Eulerian time series recorded at a time resolution of 3 hours. This is considered as high-frequency measurement, compared to
lower-frequency measurements done from e.g. weekly or monthly sampling. In oceanography, previous work from temperature

45 Eulerian sampling (Derot et al., 2016) on pH and carbonate dynamics (Schmitt et al., 2008; Zongo and Schmitt, 2011), as well
as works in atmospheric turbulence in the boundary-layer (Schmitt et al., 1994; Katul et al., 1995; Schmitt, 2007; Calif and
Schmitt, 2012, 2014) have shown that turbulent fluctuations at fixed points can be detected from hourly scales to a large scale
of about 3 months. This means that in agreement with the Richardson cascade theory (Richardson, 1922), there is an inertial
range where turbulence influence is present over a rather large range of scales from the largest (e.g. months) to the smallest

50 (e.g. seconds). The present data set is therefore analyzed here using methods from the field of turbulence in order to consider
~~their~~ pCO_2 scaling properties.

In the following section, the database chosen in this work is presented in section 2. Then the power spectral exponents are
given and their averaged values are discussed in section 3. Section 4 presents intermittency analysis and the discussion and
conclusion of this work are in section 5.
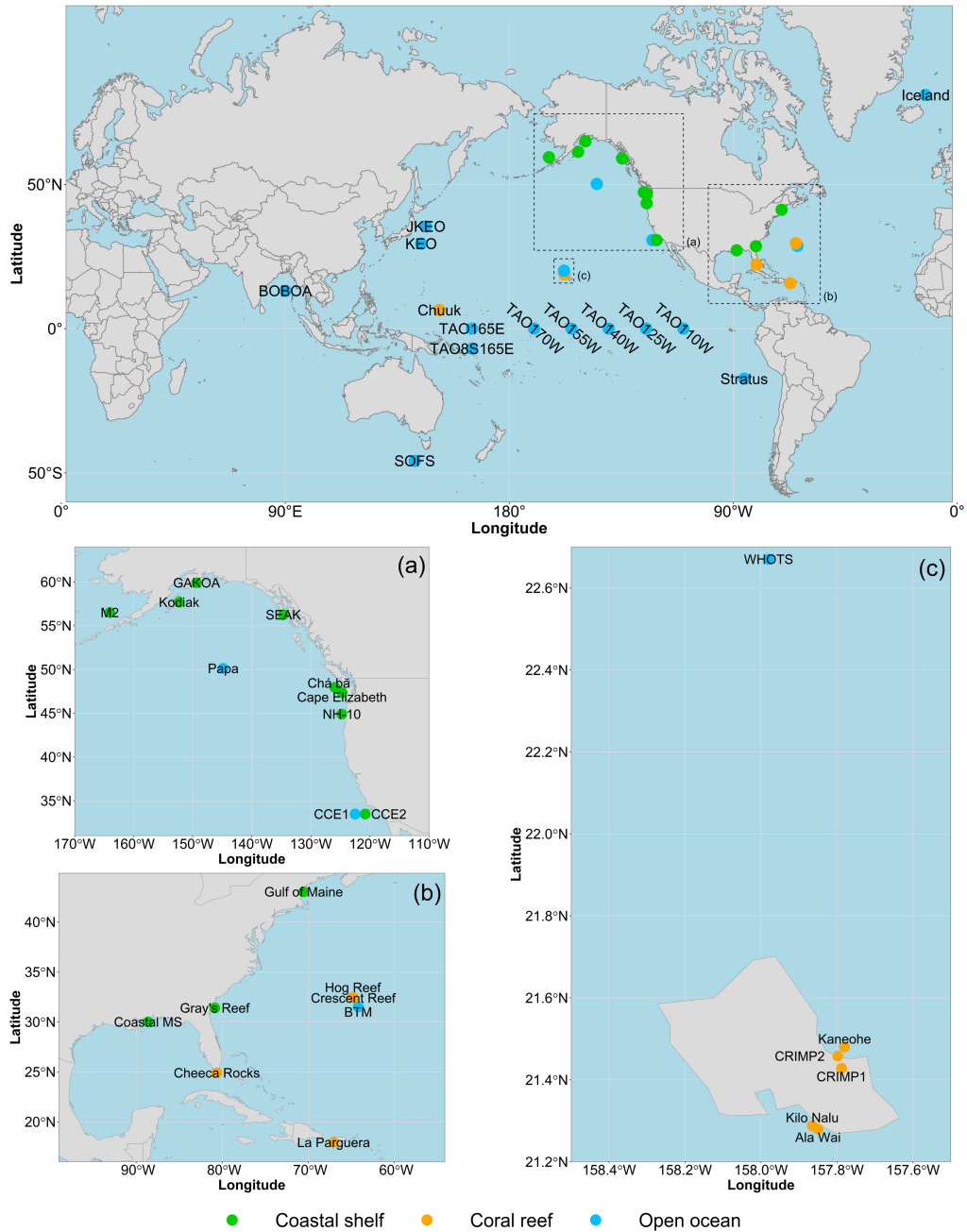
Figure 1. Maps of the position of 38 fixed position observation time series adapted from Sutton et al. (2018) with the same classification corresponding to a color code for coastal shelf buoys, coral reefs, and open ocean ecosystems.
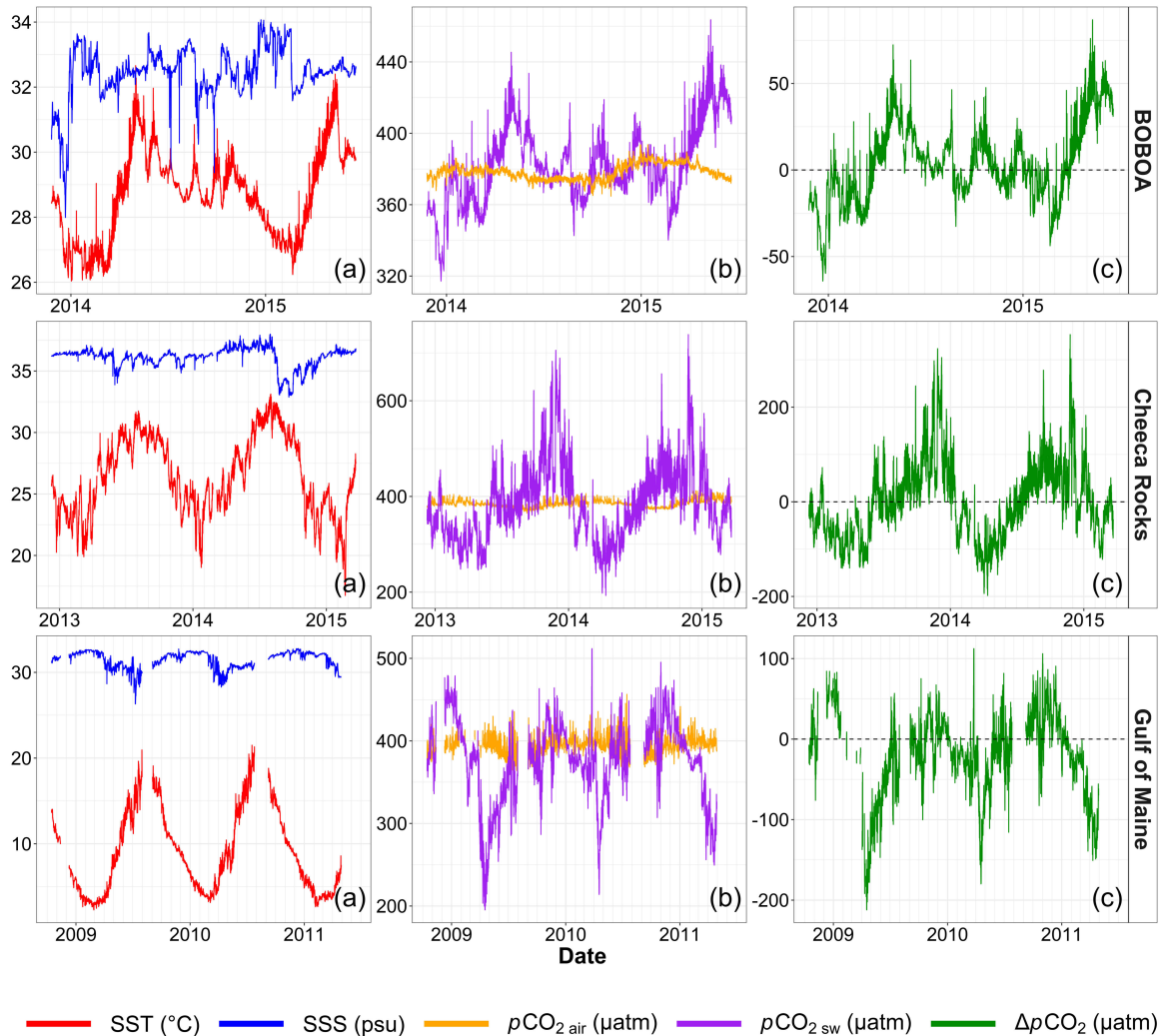
Figure 2. Portions of time series from the BOBOA (Bay of Bengal, Indian Ocean), Cheeca Rocks (Caribbean, North Atlantic Ocean) and Gulf of Maine (North Atlantic Ocean) buoys: (a) the sea surface temperature and salinity, (b) the atmospheric and oceanic pCO_2, and (c) their difference.

2 Presentation of the database

In this work, a published *in situ* observational database provided by Sutton et al. (2018, 2019) is analyzed. It contains observations from 40 fixed-point autonomous buoys distributed in the Pacific, Indian, Southern and Atlantic oceans. Two sites were discarded due to different sampling frequencies, and we have considered here 38 time series, whose locations are illustrated in Fig. 1 and are listed in the Appendix. For each buoy, the following parameters are recorded every 3 hours: sea surface

temperature (SST), sea surface salinity (SSS), seawater partial pressure of CO_2 ($pCO_{2\ sw}$) and atmospheric partial pressure of CO_2 ($pCO_{2\ air}$). SST and SSS are measured using a multiparameter sonde (Sea-Bird Electronics 16plus V2 SeaCAT or a SBE 37 MicroCAT depending on the site) in the upper layer at a depth of about 0.5 m. The pCO_2 time series are calculated from the molar fraction xCO_2 by the MAPCO$_2$ sensor, which is an optical sensor measuring the infrared absorption by the air in comparison with the infrared absorption of a reference gas. Atmospheric measures are done between 0.5 and 1 m from the sea surface (Sutton et al., 2014, 2019).

These buoys are classified by ~~the authors~~ Sutton et al. (2019) in three categories based on the type of ecosystem in which the buoy is located. In the present work, different properties according to these ecosystems are considered. Among the 38 series, there are 11 series belonging to the coastal shelf, 10 series belonging to coral reefs, and 17 series belonging to the open ocean. ~~The data paper presenting the database has~~ Sutton et al. (2019) have highlighted the appearance of anthropogenic trends and seasonality ~~(Sutton et al., 2019)~~. The database has also been used in other works: Torres et al. (2021) were interested in the mean and extreme diurnal variability of these series and have highlighted their spatial and temporal properties. These data were also used for pCO_2 data modelling purposes (Chau et al., 2022; Kwiatkowski et al., 2023).

As an example, data from 3 sites, one from each ecosystem type, are shown in Fig. 2. They correspond to the BOBOA (Bay of Bengal, open ocean), Cheeca Rocks (Gulf of Mexico, coral reefs) and Gulf of Maine (North Atlantic Ocean, coastal shelf) time series and illustrate the multiscale variability of all the studied parameters. It is also visible in this figure that for all cases the time series of $pCO_{2\ air}$ presents less relative fluctuations than $pCO_{2\ sw}$. In order to consider this property for all series, the mean, the standard deviation, and the variation coefficient (ratio of the standard deviation to the mean value) of atmospheric and oceanic ~~carbon dioxide~~ CO_2 partial pressures are estimated for all buoys. These quantities averaged for the three buoy categories are reported in Table 1. It shows that $pCO_{2\ air}$ presents much less relative fluctuations than $pCO_{2\ sw}$: the mean values are of the same order of magnitude whereas the variation coefficients are 6 to 8 times lower. For $pCO_{2\ air}$ it is between 2 and 3 % and for $pCO_{2\ sw}$ it is between 13 and 25 %. Globally, the variation coefficient for coastal shelves is larger for atmospheric series and much larger for oceanic time series. For coral reefs and open-ocean ecosystems, the mean and standard deviations are similar.

This property can be explained by the better mixing of the atmosphere (Sarmiento and Gruber, 2002). Indeed, the diffusivity coefficient of CO_2 in the atmosphere (0.16 cm^2 s^{-1} at 20.1 °C; Pritchard and Currie, 1982) is about 10,000 times higher than in the seawater (1.6·10^{-5} cm^2 s^{-1} at 20 °C; Emerson and Hamme, 2022).

Next, the difference Δ~~p~~ pCO_2 is considered. First, the conditional means and standard deviations of positive and negative values are estimated, averaged over each site of each category, and shown in Table 2. The order of magnitude of the conditional mean for positive values is of the same order for the three categories, while large variations (a ratio greater than 4) are found for the conditional average of negative values. For coral reefs and open ocean ecosystems, the overall average of positive values is much larger (almost double) than the average of negative values (in amplitude). For coastal shelf ecosystems, this proportion is reversed, and the conditional average of positive values is much smaller in amplitude than the conditional average of negative values. ~~These numbers do not directly reflect~~ The sink or source of ~~carbon dioxide~~ CO_2 of the different ecosystems~~, since it also~~ depends on the proportion of time spent in the negative or positive values: the global mean can be written as

Table 1. Statistical values based on all the raw pCO_2 time series available in Sutton et al. (2019). The mean and standard deviation values are given in μatm and variation coefficient are given in %.

Scalar	Site category	Mean $\pm\ \sigma$ (μatm)	Variation coefficient (%)
$pCO_{2\ air}$	Coastal shelf	393 ± 11	2.8
	Coral reefs	382 ± 9	2.4
	Open ocean	379 ± 9	2.4
$pCO_{2\ sw}$	Coastal shelf	348 ± 85	24.4
	Coral reefs	407 ± 53	13
	Open ocean	406 ± 55	13.5

Table 2. Conditional means, standard deviations and average proportions of positive and negative values of all the $\delta = \Delta pCO_2$ (μatm) time series averaged for each buoy site category. Conditional averages are first estimated for each time series. Then the mean and standard deviations indicated in the table are estimated from these mean values.

	Mean $\pm\ \sigma$ (μatm)		Average proportion (%)	
Site category	$\langle\delta\|\delta>0\rangle$	$-\langle\delta\|\delta<0\rangle$	$p^+ = \%_{\delta>0}$	$p^- = \%_{\delta<0}$
Coastal shelf	50 ± 37	92 ± 32	24.7	75.3
Coral reefs	52 ± 26	26 ± 19	70.0	30.0
Open ocean	49 ± 42	22 ± 18	55.1	44.9

95 $\langle\delta\rangle = p^+\langle\delta|\delta>0\rangle + p^-\langle\delta|\delta<0\rangle$. ~~It~~ Table 2 indicates that when it is a sink, globally the coastal shelf ecosystems are more active sinks compared to coral reefs or open ocean ecosystems. Concerning the proportion of negative and positive values shown in the same table, it is seen that the coastal shelf sites are much more often sinks ~~that source~~ than sources (75 % versus 25 %).~~, a proportional that is reversed for the coral reef sites~~ For the coral reefs sites, it is the opposite: they are more often sources than sinks (70 % versus 30 %). In the open ocean, there is a slight proportion in favor of sinks.

100   The probability density functions (PDF) of $\Delta_p\ pCO_2$ are also presented in Fig. 3 on a log scale. In these figures, the time series of $\Delta_p\ pCO_2$ are centered (subtraction of the mean and division by the standard deviation) and then considered globally for each ecosystem (coral reefs, open ocean, coastal shelf). A Gaussian PDF is also shown for comparison. These figures show that the difference $\Delta_p\ pCO_2$ is non-Gaussian, except for the negative values of the coastal shelf buoys. In all cases there are more large positive values than in the Gaussian law. For open ocean buoys the PDF is symmetric whereas for the two other categories it is asymmetric, with more large positive values than negative ones.
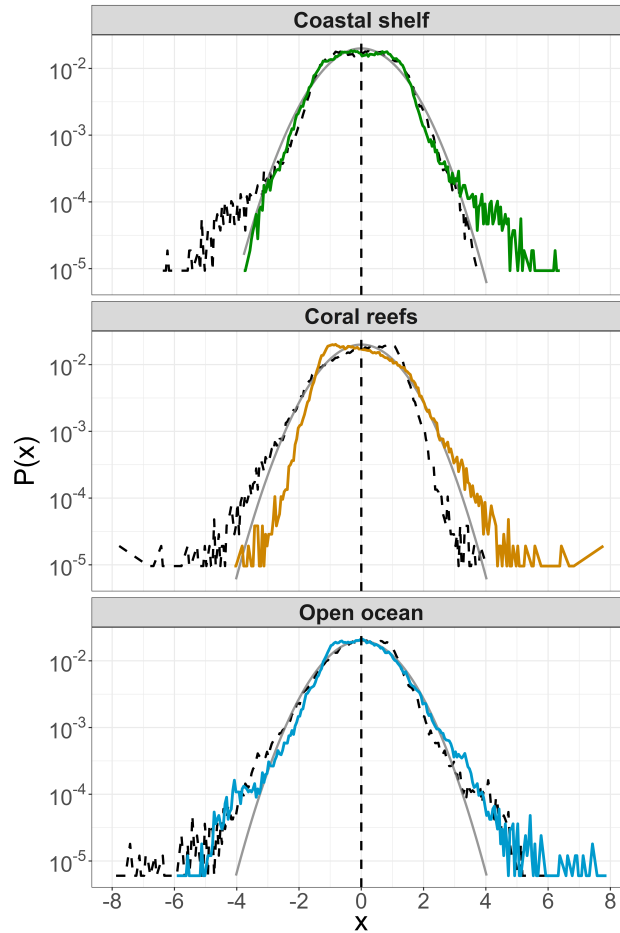
Figure 3. Probability density function (PDF) of centered time series of ΔpCO_2 considered for each site category. The black dotted lines are the symmetric PDFs and the grey continuous lines are the Gaussian PDFs. The density has been calculated using a band with of 0.05. The value represented for the x-axis is the middle value of each range.

3 Fourier spectral analysis

Fourier spectral analysis was applied to all series. Some portions of these time series have a time step shorter than 3 hours: in order to have homogeneous time steps, these portions have been averaged to have a regular sampling of 3 hours. As shown in Fig. 2, there are also large portions of missing values due to failures in measuring devices or maintenance operations. In such a case, no interpolation or averaging is performed and the following method is used. First, the autocorrelation function is estimated, which by definition can be considered only for existing data and can deal with missing values: $C(\tau) = \langle X(t)X(t+\tau)\rangle$ where X is a stationary time series with zero mean and τ is a time increment. Then the Wiener-Khinchine theorem is used

to consider the power spectrum as the Fourier transform of the autocorrelation function:

$$E(f) = \int\limits_{-\infty}^{+\infty} C(\tau) \exp(-2i\pi\tau f) \mathrm{d}\tau \qquad (2)$$

where f is the frequency and $E(f)$ the Fourier spectral density. Since time series are considered within the framework of turbulence forcing, scaling regimes are expected with the following power-law relation (Gao et al., 2021):

$$E(f) \sim f^{-\beta} \qquad (3)$$

where "$\sim$" means proportionality and $\beta > 0$ is the spectral slope. Let us recall that in homogeneous and isotropic turbulence, the famous Kolmogorov 1941 (K41) relation corresponds to a scaling law for the velocity field with a value of $\beta = 5/3$ (Kolmogorov, 1941). In such a framework, passive scalars advected by the turbulent velocity are also scaling with a scaling slope value of $\beta = 5/3$ (Obukhov, 1949; Corrsin, 1951). In the ocean, temperature and salinity are generally considered to be passive scalars advected by the turbulent velocity field; whereas other scalars can also be studied, such as dissolved oxygen, concentrations in nutrients, pH and the concentration or partial pressure of ~~carbon dioxide~~ CO_2. Other values of the spectral slope have been reported and can be interpreted as the signature of a chemical or biological activity (Seuront et al., 1996; Schmitt et al., 2008; Zongo and Schmitt, 2011).

3.1 Mean values of spectral slopes

Raw Fourier spectra can be quite noisy, preventing clear detection of scaling ranges. To prevent this, each spectrum is averaged by decade; this does not destroy spectral ~~pikes~~ peaks, but suppresses random fluctuations and provides smoother spectra. Over scaling ranges detected visually, the precise value of the spectral slope is estimated by using a least squares linear fit applied to the logarithmic values. To illustrate the scaling power spectra, the Fourier spectral plots are displayed for the three time series in Fig. 4, chosen as representative of each ecosystem: BOBOA (Bay of Bengal, open ocean), Cheeca Rocks (Gulf of Mexico, coral reefs) and Gulf of Maine (North Atlantic Ocean, coastal shelf). ~~In each case~~ In most cases, the scaling is found from the smallest scale (3 hours to a large scale of 1 year). ~~Pikes~~ Peaks are found in many cases for the annual cycle, and also for the daily and 12 hour time scales, the latter potentially corresponding to the tidal influence. The amplitude of the ~~pikes~~ peaks is not the same for each series. In some cases (i.e. salinity), the scaling at high frequency is not found below the daily time scale.

As shown in these figures, the values of the spectral slopes are variable in the range of ~~0.7~~ 0.7 to ~~1.68~~ 2.26 depending on the time series. This is performed for all 38×5 series: a spectral slope is extracted in each case, and finally the mean and standard deviations estimated over series of both ecosystems are given in Table 3. It is found that the SST is the scalar with the lowest standard deviation in spectral slopes. The averaged SST spectral slope is also close to the value 5/3, the theoretical value expected in the case of homogeneous and isotropic turbulence. Only in few cases the SST spectral slopes is much smaller than 5/3: for TAO8S165E and Kaneohe. ~~Only in few cases the SST spectral slopes is much smaller than 5/3: for M2, Coastal MS and Kaneohe. Different explanations can be given for this. First, M2 is an Alaskan buoy where ice is seasonal (Jin et al., 2007; Stabeno et al., 2010). This phenomenon could be the origin of a peculiar scaling. Second, Coastal MS is a buoy located~~
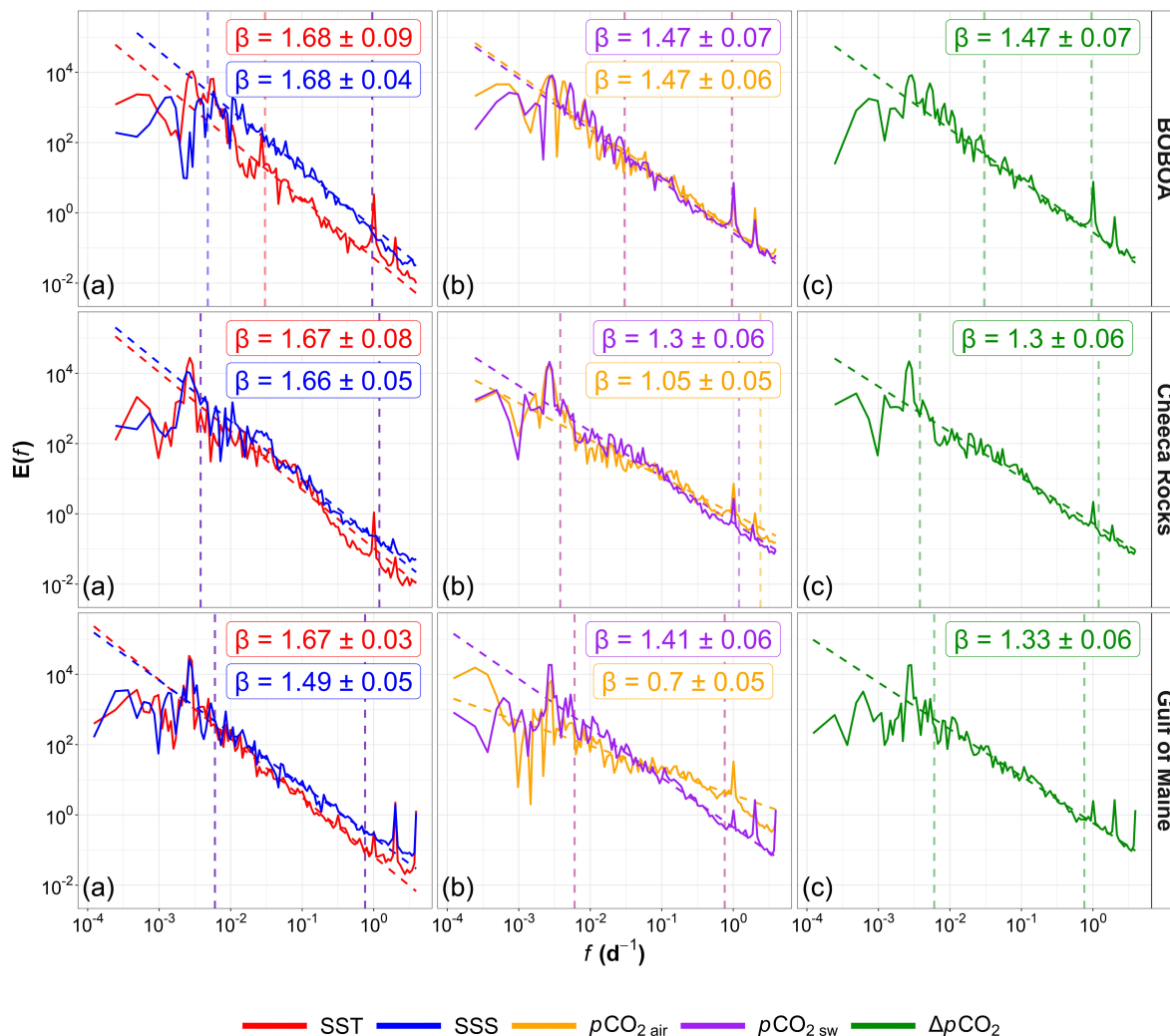
Figure 4. Fourier spectra represented in log-log for data from BOBOA (Bay of Bengal, Indian Ocean), Cheeca Rocks (Caribbean, North Atlantic Ocean) and Gulf of Maine (North Atlantic Ocean) buoys (see Fig. 2). The dotted lines represent the power-law fits and the slopes are given in each figure for (a) SST and SSS, (b) atmospheric and oceanic $p\text{CO}_2$ and (c) their difference. The horizontal dashed lines represent the range used for the estimation of the slope.

145 ~~in the Mississippi Delta. Rivers can influence the physicochemical parameters of coastal waters, such as temperature, salinity (Crossland et al., 2005; Walker et al., 2005) and also *p*CO₂ (Kealoha et al., 2020). Thirdly, Kaneohe is situated in Kaneohe Bay (Hawaii). In this region, the Kaneohe stream and other streams have an impact on the marine environment (Drupp et al., 2011), which could influence the spectral slope of the temperature field.~~ The mean spectral slopes for the other scalars are less than

5/3. The mean values for SSS, seawater pCO_2 and ΔpCO_2 are close to each other. For the atmospheric pCO_2, the averaged spectral slope is the lowest. These differences in spectral slopes could be due to biological or chemical activity.

Table 3. Mean and strandard deviations of spectral slopes for all 5 parameters, estimated for the 38 global time series.

Scalar	Mean $\pm \sigma$
SST	~~1.61~~ 1.65 $\pm$ ~~0.17~~ 0.07
SSS	~~1.35~~ 1.45 $\pm$ ~~0.29~~ 0.20
$pCO_{2\ air}$	~~1.18~~ 1.22 $\pm$ ~~0.31~~ 0.36
$pCO_{2\ sw}$	~~1.34~~ 1.37 $\pm$ ~~0.22~~ 0.21
ΔpCO_2	~~1.32~~ 1.36 $\pm$ ~~0.2~~ 0.19

150   The scaling properties of atmospheric CO_2 have been reported in previous work. Spectral slopes close to $5/3$ have been found at high frequencies (typically for scales smaller than a few seconds, from 0.2 to 10 or 25 Hz) for measurements in the atmospheric boundary layer over a forest (Anderson et al., 1986), over crop surface (Anderson and Verma, 1985), over vegetated fields (Ohtaki, 1985; Gao et al., 2020), over the ocean (Ohtaki et al., 1989), or over a littoral area (Sahlée et al., 2008). A more recent study reported measurements of atmospheric CO_2 using a tower 5 meters above the ground in a continental
155 zone. Scaling properties were found for scales of 10 seconds to 15 minutes, with a scaling slope of $\beta =$1.2 (Gao et al., 2020). This value is closer to the mean value found here for this parameter. However, the scales considered in the present study are much larger than the ones used in these works and cannot be directly compared.

Figure 5 represents scatter plots of the spectral slope of some parameters. The first subfigure (Fig. 5a) shows that there is no direct link between the spectral slopes of the atmospheric and oceanic pCO_2; the central figure (Fig. 5b) demonstrates that
160 there is a direct link between the spectral slope of the marine measurements and of the difference ΔpCO_2: this comes from the fact that, as seen above, the atmospheric measurements display much less relative fluctuations, so that the oceanic fluctuations dominate in the difference ΔpCO_2. This dominance is reflected in the spectral slopes. The last plot (Fig. 5c) shows that the temperature values are very close to the theoretical value of $5/3$ obtained for homogeneous and isotropic turbulence, while SSS, which is also often assumed to be a turbulent passive scalar (Thorpe, 2005, 2007) displays scaling properties but with
165 spectral slopes which are not compatible with a turbulent passive scalar.

3.2   Analysis of spectral slopes for each ecosystem

Here statistical analysis is done over the spectral slopes of time series belonging to different ecosystems (coastal areas, coral reefs and open ocean). The different spectral slopes for all 3 ecosystems are represented as boxplots in Fig. 6; the mean values are also given in Table 4. Concerning SSS, ~~for the coastal shelf sites, there is greater variability for the spectral slopes.~~ the
170 departure from the passive scalar values is smaller for open-ocean sites. In coastal areas, the departures from a passive scalar slope could be due to coastal forcing induced by river flows associated with shallow depths (Crossland et al., 2005). Some sites in the Equatorial Pacific (coral reefs ecosystem) have slopes very different from 5/3, which could be due to the associated
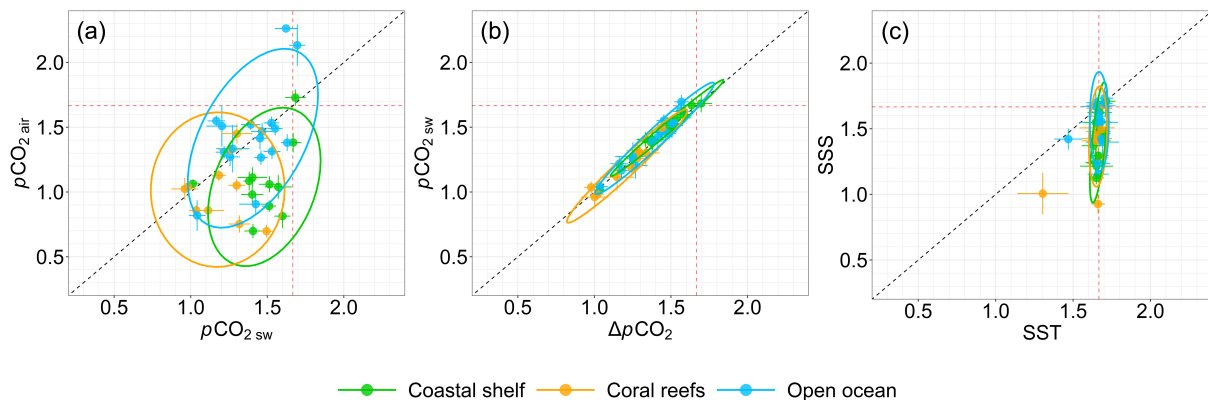
Figure 5. Scatter-plots of the Fourier spectral slopes, each dot corresponding to a given time series, and its color corresponding to the ecosystem site: (a) atmospheric versus sea water pCO_2; (b) sea water pCO_2 versus the difference ΔpCO_2 and also (c) SSS versus SST. The ellipses are calculated for each ecosystem from a 95 % confidence interval of the multivariate t-distribution. The vertical and horizontal red dotted lines represent the value 5/3. The black dotted line represents the first bisector $y = x$.

rainfall in these areas (Turk et al., 2010). For $pCO_{2\ air}$ the values for coral reefs and coastal shelf ecosystems seem similar, while for the open ocean steeper slopes are found. As mentioned above for global values, for each ecosystem, the spectral slopes for the difference ΔpCO_2 are very similar to those for $pCO_{2\ sw}$. Regarding the latter, it is visible that the spectral slopes are less steep for coral reefs sites: such a strong departure from a passive scalar could be the effect of strong biological activity in coral reefs. The ellipses shown in Fig. 5 are calculated for each ecosystem from a 95 % confidence interval of the multivariate t-distribution. They do not differentiate the ecosystems in Figs. 5a,b. ~~Only in Fig. 5c, the ellipse computed for the coastal shelf sites is clearly different from the others, an indicator of greater variability in both the SSS and SST spectral slopes~~.

Table 4. Means and standard deviations based on extracted Fourier spectral slopes β for each studied scalar and for each ecosystem.

Scalar	Coastal shelf	Coral reefs	Open ocean
SST	~~1.55~~ $1.66 \pm$ ~~0.25~~ 0.02	~~1.6~~ $1.63 \pm$ ~~0.19~~ 0.11	1.66 ± 0.05
SSS	~~1.19~~ $1.41 \pm$ ~~0.3~~ 0.18	~~1.32~~ $1.36 \pm$ ~~0.32~~ 0.23	~~1.48~~ $1.53 \pm$ ~~0.19~~ 0.17
$pCO_{2\ air}$	~~1.02~~ $1.08 \pm$ ~~0.18~~ 0.28	1.02 ± 0.24	~~1.37~~ $1.44 \pm$ ~~0.3~~ 0.35
$pCO_{2\ sw}$	~~1.41~~ $1.47 \pm$ ~~0.22~~ 0.19	1.2 ± 0.17	~~1.37~~ $1.41 \pm$ ~~0.22~~ 0.18
ΔpCO_2	~~1.39~~ $1.45 \pm$ ~~0.2~~ 0.18	1.2 ± 0.16	~~1.35~~ $1.38 \pm$ ~~0.2~~ 0.16

3.3 Latitudinal variability of pCO_2 spectral slopes

The spatial variation of the spectral exponents of pCO_2 are considered in this section, for all series, regardless of the ecosystem to which they belong. Different bins of unequal length are chosen to perform averages, with approximately the same number
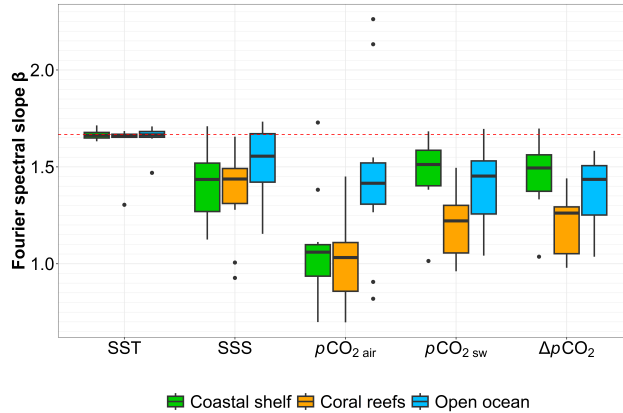
Figure 6. Representation using boxplots of all Fourier spectral slopes according to the site ecosystem (coastal shelf; coral reefs and open ocean). The horizontal dashed line corresponds to the theoretical value of 5/3 expected for passive scalars in homogeneous and isotropic turbulence. The dots signify outliers, indicating values that fall below or above the first or third quartile (respectively) by more than 1.5 times the interquartile range (distance between the first and third quartiles).

of series in each bin. The result is shown in Fig. 7 where the limits of the bins are shown as dotted lines, and the mean values for atmospheric and oceanic partial pressures in ~~carbon dioxide~~ CO_2 are displayed. The pattern is similar for both curves, with a minimal slope for tropical values (latitude around 20-30 degrees) in the northern hemisphere and an increase of the spectral slope as one moves away from this position. This latitudinal gradient can also be explained by the fact that there are more ~~buy~~ series belonging to the coral reefs ecosystem in the database for latitudes between 20°N and 30°N.

4 Multifractal intermittency

4.1 Extraction of intermittency exponents for a time series with periodicities

Turbulent time series are intermittent and possess large fluctuations on many different scales. Such fluctuations are classically studied by considering structure functions of the form $\Delta X_\tau = X(t + \tau) - X(t)$, corresponding to time increments at scale τ. The scaling intermittent properties are considered by estimating the moments of order q of the structure functions (Frisch, 1995; Schmitt and Huang, 2016):

$$\langle |\Delta X_\tau|^q \rangle \sim \tau^{\zeta(q)} \tag{4}$$

where $q > 0$ is the moment order (which can be non-integer) and $\zeta(q)$ is the scaling exponent of the corresponding moment function. Larger moments correspond to more intense fluctuations and the whole $\zeta(q)$ curve characterizes the multi-scale intermittency of the time series. The Fourier spectrum corresponds to a moment of order 2: the spectral exponent β is related with $\zeta(2)$: $\beta = 1 + \zeta(2)$.
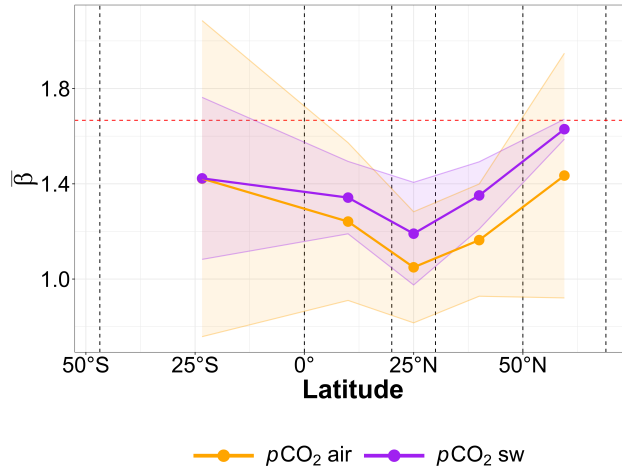
Figure 7. Average Fourier spectral slope β $\bar{\beta}$ in function of the latitude. The red dotted line represent the value 5/3. The ranges of values used for each point are represented by the black dotted lines: $[46.8°S\,;0°[$ (3 stations), $[0°\,;20°N[$ (9 stations), $[20°N\,;30°N[$ (7 stations), $[30°N\,;50°N[$ (13 stations) and $[50°N\,;69°N[$ (6 stations).

Unfortunately, the periodicity in the series, even weak, is known to destroy the scaling properties of structure functions

200 (Huang et al., 2011; Schmitt and Huang, 2016) and in this case other methods are needed to extract the scaling exponent $\zeta(q)$. This is done here in the spectral space, by using the Hilbert spectral analysis (HSA) associated with empirical mode decomposition (EMD), using the generalized HSA method. This method uses first the EMD, which is an algorithm developed to decompose the original time series into N other time series called intrinsic mode functions (IMFs; Huang et al., 1998, 1999; Flandrin et al., 2004). This signal analysis has already been used to study multi-scale variability of CO_2 time

205 series (Landschützer et al., 2016; Zhang et al., 2022). The sum of IMFs $C_i(t)$ and a residue $r_n(t)$ give the original signal $X(t)$:

$$X(t) = \sum_{i=1}^{N} C_i(t) + r_n(t) \tag{5}$$

~~Missing values are first linearly interpolated to compensate for the fact that the EMD method requires a complete signal.~~ This iterative algorithm is based on a spline interpolation of local minima and maxima. Each IMF is a zero-mean time series

210 localized in the frequency space. Their Hilbert transform is denoted $\tilde{C}_i(t)$:

$$\tilde{C}_i(t) = \frac{1}{\pi} PV \int_{-\infty}^{+\infty} \frac{C_i(\tau)}{t-\tau} \mathrm{d}\tau \tag{6}$$

where PV indicates the Cauchy principal value. The analytic signal $z_i = C_i + j\tilde{C}_i$ is a complex number that can be written as $z_i = A_i(t)e^{j\theta_i(t)}$, where $A_i(t)$ is the local amplitude and $\theta_i(t)$ the local phase of $C_i(t)$. Leaving the residual, the original signal can be rewritten as the sum of the real part of all the analytic signals z_i as $X(t) = Re \sum_{i=1}^{N} A_i(t)e^{j\theta_i(t)}$. This transformation

needs regular time steps as it done using fast Fourier transform (Huang and Schmitt, 2014). The missing data were so replaced by the value 0. Here, a local instantaneous frequency is extracted from $\omega = d\theta/dt$ (where the phase $\theta(t)$ is given by $\theta_i(t) = \tan^{-1}\tilde{C}_i(t)/C_i(t)$). When we have the instantaneous frequency information, missing data parts are then excluded in the following steps. A joint probability density function of frequency and amplitude $p(\omega, A)$ is extracted from the data and a Hilbert power spectrum is computed as $L_2(\omega) = \int_0^{+\infty} p(\omega, A)A^2 dA$. This Hilbert spectrum is similar to the Fourier spectrum $E(f)$ (Huang et al., 2008). To consider the intermittency of the signal in the EMD-HSA framework, the Hilbert marginal spectrum $L_q(\omega)$ is calculated for different statistical moments q (Huang et al., 2008, 2011; Schmitt and Huang, 2016) as $L_q(\omega) = \int_0^{+\infty} p(\omega, A)A^q dA$. For scaling time series, it has been shown that this can be written as:

$$L_q(\omega) \sim \omega^{-\xi(q)} \tag{7}$$

for frequencies belonging to the scaling range, where the scaling exponent in the amplitude-frequency space $\xi(q)$ is related to the structure functions scaling exponents (also called scaling moment function) as $\zeta(q) = \xi(q) - 1$. It was previously shown using simulations that this EMD-HSA approach, with the estimation of multifractal exponents in the frequency space, is not affected by the periodicity in the original series (Huang et al., 2011).

This method is applied here to the time series to extract intermittency exponents. There are several intermittency models published in the literature (Schmitt and Huang, 2016). The classical one is the lognormal model originally proposed by Kolmogorov (Kolmogorov, 1962). This model provides a quadratic expression which is chosen here as a fit of the nonlinear curve of the $\zeta(q)$ function. In this framework the scaling exponent can be written as $\zeta(q) = qH - K(q)$ where $H = \zeta(1)$ is the Hurst exponent (usually $0 \le H \le 1$) and $K(q)$ captures the intermittency corrections. In the lognormal framework, only one more parameter is needed here, the intermittency parameters $\mu = K(2) = 2H - \zeta(2)$. These two parameters are extracted from the EMD-HSA exponents $\xi(q)$.

4.2 Intermittency analysis of the database

The EMD-HSA method has been applied here only to 28 stations among the 38 studied stations: for the remaining 10 stations (8 coral reefs and 2 open ocean sites) the scaling of moments of order larger than 2 was destroyed due to a too low number of data points in the series. The results for the 3 specific stations chosen as representative of the three ecosystems are shown in Fig. 8, for moments from 0 to 4. The shape of scaling exponent $\zeta(q)$ is concave as expected. Some scaling exponents are almost linear, which means that the intermittency correction is weak. The overall nonlinear and concave shapes are captured by the two parameters H and μ. The larger μ, the more important the intermittency corrections are. These parameters are estimated for each series, and their mean and standard deviation are provided in Table 5. The values of H are estimated from the first-order moment using the EMD-HSA method, whereas the values of the spectral slopes β are estimated using Fourier analysis: this means that there may be some slight differences due to the method and intermittency corrections, but globally the relation $\beta \simeq 1 + 2H$ is approximately valid.

Concerning the intermittency parameter, let us note that if the same procedure is applied to the velocity and passive scalar in fully developed hydrodynamic turbulence ($H = \zeta(1)$ and $\mu = 2\zeta(1) - \zeta(2)$), we obtain values of $H = 0.37$ and $\mu = 0.04$
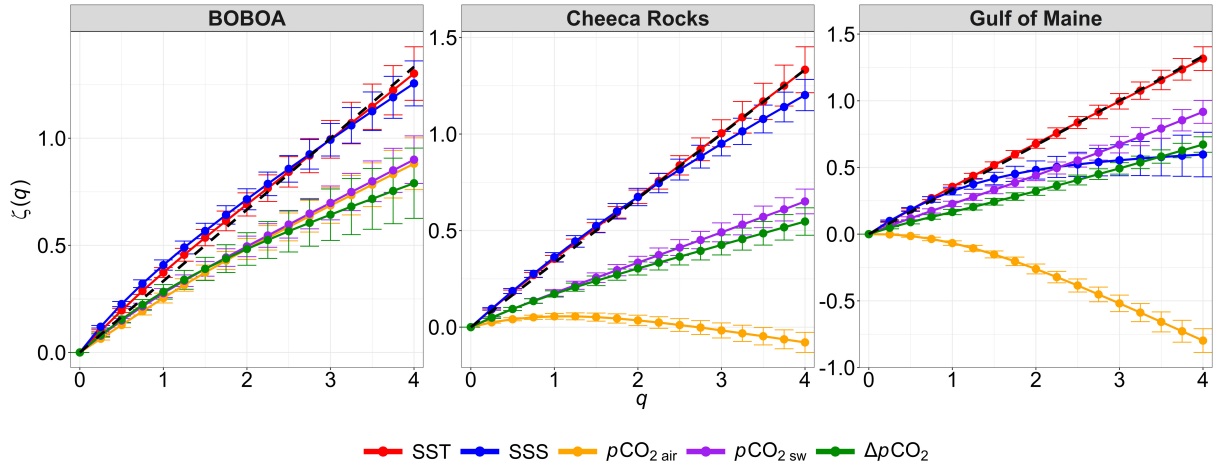
Figure 8. Scaling moment function $\zeta(q) = \xi(q) - 1$ of the BOBOA, Cheeca Rocks and Gulf of Maine buoys time series for different statistical moments q from 0 to 4. The dashed line represents the theoretical relation $q/3$ linked to a monofractal dynamics with $H = 1/3$ as in homogeneous and isotropic turbulence with no intermittency.

for the velocity field (Schmitt, 2006) and $H = 0.38$ and $\mu = 0.12$ for the passive scalar field (Schmitt et al., 1996). The values found here for μ are of the same order of magnitude, and sometimes slightly smaller than what is found for the passive scalar in hydrodynamic turbulence. The results obtained show also that overall, the intermittency parameter is greater for the salinity and atmospheric partial pressure of ~~carbon dioxide~~ CO_2. It also shows for the first time the multifractal intermittency of oceanic and atmospheric pCO_2 fields.

Table 5. For all 5 parameters, the Hurst index H and the intermittency parameters μ: mean and standard deviations estimated for the 28 time series. For homogeneous and isotropic turbulence, the expected value for H is $1/3$ with an experimental intermittency parameter $\mu \simeq 0.04$.

Scalar	H	μ
SST	~~0.35~~ 0.36 ± 0.03	~~0.03~~ 0.04 ± ~~0.03~~ 0.04
SSS	~~0.36~~ 0.30 ± ~~0.15~~ 0.09	~~0.08~~ 0.09 ± 0.07
pCO_2 air	~~0.22~~ 0.21 ± ~~0.17~~ 0.16	~~0.06~~ 0.08 ± ~~0.06~~ 0.07
pCO_2 sw	~~0.27~~ 0.26 ± ~~0.07~~ 0.08	~~0.03~~ 0.08 ± ~~0.03~~ 0.11
ΔpCO_2	~~0.28~~ 0.24 ± ~~0.08~~ 0.08	~~0.03~~ 0.06 ± ~~0.03~~ 0.09

5 Discussion and conclusion

Here a published database of high-frequency fixed point buoys recorded at 3 hours resolution has been considered. The dynamics of ~~sea surface salinity, sea surface temperature~~ sea surface temperature, sea surface salinity, seawater and atmospheric

partial pressure of ~~carbon dioxide~~ CO_2 and the difference ΔpCO_2 have been considered for each site. These ~~quantifies~~ quantities are scalars forced and transported by turbulence; they display large turbulent-like fluctuations ~~in~~ at many different scales and their multiscale dynamics have been considered ~~on multiscale~~ by ~~estimating the scaling properties~~ using the Fourier transform: it was found that these series have scaling properties from the smallest scale (3 hours) to one year. Mean spectral slopes have been estimated: the SST possessed spectral slopes on average close to the value of $5/3$ corresponding to 3D passive scalars in homogeneous and isotropic turbulence. The other scalars displayed values of the spectral slope β much smaller, from about ~~1.2~~ 1.22 to ~~1.35~~ 1.45, indicating a behaviour different from a purely passive scalar of turbulence. Such values have already been found for other scalars (fluorescence, pH) in marine waters for the same range of scales (Seuront et al., 1996; Schmitt et al., 2008; Zongo and Schmitt, 2011). Mean values were also estimated in average for different ecosystems (coastal shelf, coral reefs and the open ocean) and some differences could be detected. There were also latitudinal variations in these slopes.

The Kolmogorov-Obukhov-~~Corrsing~~ Corrsin slope of 5/3 for passive scalars was obtained through dimensional analysis. Let us emphasize here that similar theoretical explanations for the slopes close to 6/5, 4/3 or 5/2 for the scalars considered are not presently available; in future works dimensional analysis could be explored in this framework.

Power spectra correspond to second-order moments and medium fluctuations. To study the intermittent and multifractal properties of the series, the EMD-HSA method was used, since the classical structure function approach cannot be used for series possessing periodicity as is the case here, with daily and tidal forcing. This approach could not be used for all series since it needs rather large datasets. It was used for 28 series and the multifractal properties were characterized by considering a lognormal fit, with the estimation of the Hurst exponent H and the intermittency parameter μ. This showed that in general, the different time series possess multifractal properties with various intensity of the intermittency exponent (the largest being found in SSS and ~~atmospheric~~ pCO_2). We may note also that the approach used here is consistent with previous works involving singular spectra analysis and assumptions of multifractality for oceanic pCO_2 data (Hernández-Carrasco et al., 2015, 2018).

Considering pCO_2 series, one of the interesting points in the present time series is the fact that simultaneous measurements of atmospheric and oceanic pCO_2 are estimated. It was found that the variation coefficient of atmospheric pCO_2 (ratio of standard deviation to the mean) is much lower than for the marine waters with a ratio of 6 to 8. Furthermore, the difference ΔpCO_2 was studied here ~~and shown to be scaling and multifractal~~ and to the best of our knowledges, it is the first time that this quantity is shown to have multifractal properties. In the framework of the log-normal multifractal model, we have provided the two parameters $H = 0.24$ and $\mu = 0.06$. These parameters characterize the intermittency of the CO_2 flux between air and water on the range of scales which was considered here, i.e. in average between days and 1 year. This is clearly related to turbulent forcing. Since the direction of the flux and the fact that a given site is a sink or a source of CO_2, is given by the difference ΔpCO_2, such turbulent forcing is an important point for future studies: (i) perform the same analysis at smaller scales using higher resolution measurements; (ii) see more precisely how the turbulent forcing influences the sign of the difference, and (iii) how the intermittency properties of these differences is related with the forcing and the climate of a given site. The influence of the ecosystem found here for some average values of the parameter β is a first step in this direction.

290 *Code and data availability.* Data are freely accessible in Sutton et al. (2018, 2019, https://doi.org/10.5194/essd-11-421-2019). Modified data from this study are available upon request. The code for the Fourier spectral analyzes is published in Gao et al. (2021).

Author contributions. FGS directed the research and KR performed the code and the analysis. YH helped with the code development and the finalization of the results. KR wrote the first draft and all authors revised and edited the manuscript.

Competing interests. The authors declare that no competing interests are present.

295 *Acknowledgements.* The Région Hauts-de-France and the ANR project CO_2Coast (P.I. Hubert Loisel, ANR-20-CE01-0021) are acknowledged for cofunding of the PhD thesis of KR.

Appendix A: Summary of the database

Table A1 contains information about the complete used database: location, category, time coverage, size and proportions of missing data.

Table A1. Summary table of all the time series in the database studied (Sutton et al., 2019). The time resolution for each of these time series is 3 hours.

Station	Lat	Long	Category	Start date	End date	Size	SST	SSS	$p\mathrm{CO}_{2\,sw}$	$p\mathrm{CO}_{2\,air}$	$\Delta p\mathrm{CO}_2$
							% of missing data				
Cape Elizabeth	47.353	-124.731	Coastal shelf	23/06/2006 06:00	30/10/2015 00:00	27,327	33.29	34.54	35.27	34.76	35.42
CCE2	33.479	-120.814	Coastal shelf	17/01/2010 18:00	28/04/2015 00:00	15,411	13.6	13.61	13.91	14.05	14.27
Chá bă	47.963	-125.958	Coastal shelf	17/07/2010 12:00	09/12/2016 09:00	18,696	49.23	51.24	49.47	49.56	49.61
Coastal MS	30	-88.6	Coastal shelf	12/05/2009 21:00	30/03/2015 15:00	17,183	70	70	70.08	70.1	70.13
GAKOA	59.91	-149.35	Coastal shelf	19/05/2011 21:00	20/01/2017 21:00	16,585	25.63	25.63	25.72	25.88	25.9
Gray's Reef	31.4	-80.87	Coastal shelf	18/07/2006 09:00	15/10/2015 12:00	27,010	30.55	34.03	39.8	34.25	39.82
Gulf of Maine	43.023	-70.542	Coastal shelf	29/08/2007 03:00	03/11/2015 15:00	23,909	28.57	28.58	29.32	33.31	33.41
Kodiak	57.7	-152.31	Coastal shelf	30/03/2013 00:00	18/04/2016 18:00	8,927	7.11	7.11	7.29	7.36	7.38
M2	56.51	-164.04	Coastal shelf	06/05/2013 06:00	29/05/2016 21:00	8,958	58.26	58.26	58.57	58.58	58.77
NH-10	44.904	-124.778	Coastal shelf	03/04/2014 09:00	28/09/2015 18:00	4,348	36.02	36.02	41.86	36.32	42.04
SEAK	56.26	-134.67	Coastal shelf	29/03/2013 03:00	22/07/2014 06:00	3,842	22.93	22.93	23.48	23.35	23.61
Ala Wai	21.28	-157.85	Coral reefs	07/06/2008 00:00	28/07/2014 18:00	17,943	26.1	26.1	26.48	26.39	26.71
Cheeca Rocks	24.91	-80.624	Coral reefs	08/12/2011 21:00	03/05/2016 12:00	12,862	16.25	16.28	16.47	16.54	16.57
Chuuk	7.46	151.9	Coral reefs	18/11/2011 12:00	28/11/2015 00:00	11,765	4.28	4.28	4.75	4.75	4.81
Crescent Reef	32.4	-64.79	Coral reefs	27/11/2010 03:00	07/07/2015 15:00	13,469	21.69	21.69	21.81	21.82	21.83
CRIMP1	21.428	-157.788	Coral reefs	01/12/2005 03:00	30/05/2008 21:00	7,295	26.1	26.18	26.66	26.68	26.81
CRIMP2	21.458	-157.798	Coral reefs	11/06/2008 00:00	11/03/2013 09:00	13,876	18.52	18.52	19.92	18.67	20.06
Hog Reef	32.46	-64.83	Coral reefs	05/12/2010 03:00	07/01/2015 09:00	11,955	40.61	40.61	40.69	40.65	40.7
Kaneohe	21.48	-157.78	Coral reefs	30/09/2011 03:00	10/10/2016 09:00	14,699	47.79	52.96	53.16	53.13	53.18
Kilo Nalu	21.288	-157.865	Coral reefs	07/06/2008 18:00	02/02/2017 18:00	25,297	59.57	59.57	59.62	59.81	59.83
La Parguera	17.954	-67.051	Coral reefs	16/01/2009 21:00	11/01/2017 12:00	23,334	20.73	20.75	21.67	21.71	21.74
BOBOA	15	90	Open ocean	25/11/2013 15:00	09/01/2017 03:00	9,125	22.9	22.9	23.36	23.2	23.36
BTM	31.5	-64.2	Open ocean	22/10/2005 00:00	01/10/2007 12:00	5,677	11.82	11.87	12.7	12.08	12.74
CCE1	33.48	-122.51	Open ocean	11/11/2008 18:00	26/10/2014 03:00	17,396	45.52	45.52	45.96	45.66	45.97
Iceland	68	-12.67	Open ocean	17/08/2013 03:00	02/11/2014 12:00	3,540	30.23	30.23	30.59	32.01	32.01
JKEO	37.93	146.52	Open ocean	20/02/2007 12:00	03/10/2007 18:00	1,803	0.06	34.83	49.08	48.25	49.25
KEO	32.28	144.58	Open ocean	26/09/2007 21:00	12/08/2015 00:00	23,010	18.04	18.35	20.93	18.57	20.99
Papa	50.13	-144.84	Open ocean	09/06/2007 21:00	16/06/2015 15:00	23,431	20.59	22.37	23.31	22.55	23.34
SOFS	-46.8	142	Open ocean	25/11/2011 06:00	15/10/2013 00:00	5,519	31.89	31.89	33	32.43	33.34
Stratus	-19.7	-85.6	Open ocean	19/10/2006 21:00	03/04/2015 03:00	24,699	15.84	15.86	22.83	22.85	22.88
TAO110W	0	-110	Open ocean	20/09/2009 06:00	03/06/2017 03:00	22,504	57.84	57.75	63.62	60.57	63.62
TAO125W	0	-125	Open ocean	16/03/2005 03:00	06/02/2017 03:00	34,761	45.55	49.45	55.98	52.98	55.98
TAO140W	0	-140	Open ocean	23/05/2004 06:00	22/03/2015 15:00	31,644	40.74	50.37	55.12	41.63	55.12
TAO155W	0	-155	Open ocean	14/01/2010 15:00	17/11/2014 18:00	14,146	48.13	73.19	74.27	73.6	74.27
TAO165E	0	165	Open ocean	24/02/2010 00:00	03/02/2013 00:00	8,601	41.25	63.26	72.48	69.7	72.48
TAO170W	0	-170	Open ocean	05/07/2005 00:00	15/05/2012 21:00	20,056	35.51	35.51	41.79	36.16	41.82
TAO8S165E	-8	165	Open ocean	23/06/2009 03:00	15/11/2011 09:00	7,003	4.4	13.85	14.61	14.29	14.62
WHOTS	22.67	-157.98	Open ocean	20/12/2004 15:00	15/07/2015 00:00	30,868	29.29	28.13	30.72	30.13	30.84

300 **References**

Alola, A. A. and Kirikkaleli, D.: Global Evidence of Time-Frequency Dependency of Temperature and Environmental Quality from a Wavelet Coherence Approach, Air Quality, Atmosphere & Health, 14, 581–589, https://doi.org/10.1007/s11869-020-00962-z, 2021.

Anderson, D. E. and Verma, S. B.: Turbulence Spectra of CO_2, Water Vapor, Temperature and Wind Velocity Fluctuations over a Crop Surface, Boundary-Layer Meteorology, 33, 1–14, https://doi.org/10.1007/BF00137033, 1985.

305 Anderson, D. E., Verma, S. B., Clement, R. J., Baldocchi, D. D., and Matt, D. R.: Turbulence Spectra of CO_2, Water Vapor, Temperature and Velocity over a Deciduous Forest, Agricultural and Forest Meteorology, 38, 81–99, https://doi.org/10.1016/0168-1923(86)90051-1, 1986.

Anderson, T. R., Hawkins, E., and Jones, P. D.: CO_2, the Greenhouse Effect and Global Warming: From the Pioneering Work of Arrhenius and Callendar to Today's Earth System Models, Endeavour, 40, 178–187, https://doi.org/10.1016/j.endeavour.2016.07.002, 2016.

Calif, R. and Schmitt, F. G.: Modeling of Atmospheric Wind Speed Sequence Using a Lognormal Continuous Stochastic Equation, Journal

310 of Wind Engineering and Industrial Aerodynamics, 109, 1–8, https://doi.org/10.1016/j.jweia.2012.06.002, 2012.

Calif, R. and Schmitt, F. G.: Multiscaling and Joint Multiscaling Description of the Atmospheric Wind Speed and the Aggregate Power Output from a Wind Farm, Nonlinear Processes in Geophysics, 21, 379–392, https://doi.org/10.5194/npg-21-379-2014, 2014.

Chau, T. T. T., Gehlen, M., and Chevallier, F.: A Seamless Ensemble-Based Reconstruction of Surface Ocean pCO_2 and Air–Sea CO_2 Fluxes over the Global Coastal and Open Oceans, Biogeosciences, 19, 1087–1109, https://doi.org/10.5194/bg-19-1087-2022, 2022.

315 Corrsin, S.: On the Spectrum of Isotropic Temperature Fluctuations in an Isotropic Turbulence, Journal of Applied Physics, 22, 469–473, https://doi.org/10.1063/1.1699986, 1951.

Crisp, D., Dolman, H., Tanhua, T., McKinley, G. A., Hauck, J., Bastos, A., Sitch, S., Eggleston, S., and Aich, V.: How Well Do We Understand the Land-Ocean-Atmosphere Carbon Cycle?, Reviews of Geophysics, 60, e2021RG000 736, https://doi.org/10.1029/2021RG000736, 2022.

320 Crossland, C. J., Baird, D., Ducrotoy, J.-P., Lindeboom, H., Buddemeier, R. W., Dennison, W. C., Maxwell, B. A., Smith, S. V., and Swaney, D. P.: The Coastal Zone — a Domain of Global Interactions, in: Coastal Fluxes in the Anthropocene: The Land-Ocean Interactions in the Coastal Zone Project of the International Geosphere-Biosphere Programme, edited by Crossland, C. J., Kremer, H. H., Lindeboom, H. J., Marshall Crossland, J. I., and Le Tissier, M. D. A., Global Change — The IGBP Series, pp. 1–37, Springer, Berlin, Heidelberg, 2005.

De La Rocha, C. L. and Passow, U.: The Biological Pump, in: Treatise on Geochemistry (Second Edition), edited by Holland, H. D. and

325 Turekian, K. K., pp. 93–122, Elsevier, Oxford, 2014.

Derot, J., Schmitt, F. G., Gentilhomme, V., and Morin, P.: Correlation between Long-Term Marine Temperature Time Series from the Eastern and Western English Channel: Scaling Analysis Using Empirical Mode Decomposition, Comptes Rendus Geoscience, 348, 343–349, https://doi.org/10.1016/j.crte.2015.12.001, 2016.

Emerson, S. R. and Hamme, R. C.: Chemical Oceanography, Cambridge University Press, 2022.

330 Falkowski, P., Scholes, R. J., Boyle, E., Canadell, J., Canfield, D., Elser, J., Gruber, N., Hibbard, K., Högberg, P., Linder, S., Mackenzie, F. T., Moore III, B., Pedersen, T., Rosenthal, Y., Seitzinger, S., Smetacek, V., and Steffen, W.: The Global Carbon Cycle: A Test of Our Knowledge of Earth as a System, Science, 290, 291–296, https://doi.org/10.1126/science.290.5490.291, 2000.

Flandrin, P., Rilling, G., and Goncalves, P.: Empirical Mode Decomposition as a Filter Bank, IEEE Signal Processing Letters, 11, 112–114, https://doi.org/10.1109/LSP.2003.821662, 2004.

335 Friedlingstein, P., O'Sullivan, M., Jones, M. W., Andrew, R. M., Bakker, D. C. E., Hauck, J., Landschützer, P., Le Quéré, C., Luijkx, I. T., Peters, G. P., Peters, W., Pongratz, J., Schwingshackl, C., Sitch, S., Canadell, J. G., Ciais, P., Jackson, R. B., Alin, S. R., Anthoni, P., Barbero, L., Bates, N. R., Becker, M., Bellouin, N., Decharme, B., Bopp, L., Brasika, I. B. M., Cadule, P., Chamberlain, M. A., Chandra, N., Chau, T.-T.-T., Chevallier, F., Chini, L. P., Cronin, M., Dou, X., Enyo, K., Evans, W., Falk, S., Feely, R. A., Feng, L., Ford, D. J., Gasser, T., Ghattas, J., Gkritzalis, T., Grassi, G., Gregor, L., Gruber, N., Gürses, Ö., Harris, I., Hefner, M., Heinke, J., Houghton, R. A.,

340 Hurtt, G. C., Iida, Y., Ilyina, T., Jacobson, A. R., Jain, A., Jarníková, T., Jersild, A., Jiang, F., Jin, Z., Joos, F., Kato, E., Keeling, R. F.,

Kennedy, D., Klein Goldewijk, K., Knauer, J., Korsbakken, J. I., Körtzinger, A., Lan, X., Lefèvre, N., Li, H., Liu, J., Liu, Z., Ma, L., Marland, G., Mayot, N., McGuire, P. C., McKinley, G. A., Meyer, G., Morgan, E. J., Munro, D. R., Nakaoka, S.-I., Niwa, Y., O'Brien, K. M., Olsen, A., Omar, A. M., Ono, T., Paulsen, M., Pierrot, D., Pocock, K., Poulter, B., Powis, C. M., Rehder, G., Resplandy, L., Robertson, E., Rödenbeck, C., Rosan, T. M., Schwinger, J., Séférian, R., Smallman, T. L., Smith, S. M., Sospedra-Alfonso, R., Sun, Q., Sutton, A. J., Sweeney, C., Takao, S., Tans, P. P., Tian, H., Tilbrook, B., Tsujino, H., Tubiello, F., van der Werf, G. R., van Ooijen, E., Wanninkhof, R., Watanabe, M., Wimart-Rousseau, C., Yang, D., Yang, X., Yuan, W., Yue, X., Zaehle, S., Zeng, J., and Zheng, B.: Global Carbon Budget 2023, Earth System Science Data, 15, 5301–5369, https://doi.org/10.5194/essd-15-5301-2023, 2023.

Frisch, U.: Turbulence: The Legacy of A. N. Kolmogorov, Cambridge University Press, 1995.

Gao, Y., Schmitt, F. G., Hu, J., and Huang, Y.: Scaling Analysis of the China France Oceanography Satellite Along-Track Wind and Wave Data, Journal of Geophysical Research: Oceans, 126, e2020JC017 119, https://doi.org/10.1029/2020JC017119, 2021.

Gao, Z., Liu, H., Arntzen, E., Mcfarland, D. P., Chen, X., and Huang, M.: Uncertainties in Turbulent Statistics and Fluxes of CO_2 Associated With Density Effect Corrections, Geophysical Research Letters, 47, e88 859, https://doi.org/10.1029/2020GL088859, 2020.

Henson, S., Le Moigne, F., and Giering, S.: Drivers of Carbon Export Efficiency in the Global Ocean, Global Biogeochemical Cycles, 33, 891–903, https://doi.org/10.1029/2018GB006158, 2019.

Hernández-Carrasco, I., Sudre, J., Garçon, V., Yahia, H., Garbe, C., Paulmier, A., Dewitte, B., Illig, S., Dadou, I., González-Dávila, M., and Santana-Casiano, J. M.: Reconstruction of Super-Resolution Ocean pCO_2 and Air–Sea Fluxes of CO_2 from Satellite Imagery in the Southeastern Atlantic, Biogeosciences, 12, 5229–5245, https://doi.org/10.5194/bg-12-5229-2015, 2015.

Hernández-Carrasco, I., Garçon, V., Sudre, J., Garbe, C., and Yahia, H.: Increasing the Resolution of Ocean pCO_2 Maps in the South Eastern Atlantic Ocean Merging Multifractal Satellite-Derived Ocean Variables, IEEE Transactions on Geoscience and Remote Sensing, 56, 6596–6610, https://doi.org/10.1109/TGRS.2018.2840526, 2018.

Huang, N. E., Shen, Z., Long, S. R., Wu, M. C., Shih, H. H., Zheng, Q., Yen, N.-C., Tung, C. C., and Liu, H. H.: The Empirical Mode Decomposition and the Hilbert Spectrum for Nonlinear and Non-Stationary Time Series Analysis, Proceedings of the Royal Society of London. Series A: Mathematical, Physical and Engineering Sciences, 454, 903–995, https://doi.org/10.1098/rspa.1998.0193, 1998.

Huang, N. E., Shen, Z., and Long, S. R.: A NEW VIEW OF NONLINEAR WATER WAVES: The Hilbert Spectrum[1], Annual Review of Fluid Mechanics, 31, 417–457, https://doi.org/10.1146/annurev.fluid.31.1.417, 1999.

Huang, Y. and Schmitt, F. G.: Time Dependent Intrinsic Correlation Analysis of Temperature and Dissolved Oxygen Time Series Using Empirical Mode Decomposition, Journal of Marine Systems, 130, 90–100, https://doi.org/10.1016/j.jmarsys.2013.06.007, 2014.

Huang, Y. X., Schmitt, F. G., Lu, Z. M., and Liu, Y. L.: An Amplitude-Frequency Study of Turbulent Scaling Intermittency Using Empirical Mode Decomposition and Hilbert Spectral Analysis, Europhysics Letters, 84, 40 010, https://doi.org/10.1209/0295-5075/84/40010, 2008.

Huang, Y. X., Schmitt, F. G., Hermand, J.-P., Gagne, Y., Lu, Z. M., and Liu, Y. L.: Arbitrary-Order Hilbert Spectral Analysis for Time Series Possessing Scaling Statistics: Comparison Study with Detrended Fluctuation Analysis and Wavelet Leaders, Physical Review E, 84, 016 208, https://doi.org/10.1103/PhysRevE.84.016208, 2011.

Katul, G. G., Chu, C. R., Parlange, M. B., Albertson, J. D., and Ortenburger, T. A.: Low-Wavenumber Spectral Characteristics of Velocity and Temperature in the Atmospheric Surface Layer, Journal of Geophysical Research: Atmospheres, 100, 14 243–14 255, https://doi.org/10.1029/94JD02616, 1995.

Keenan, T., Baker, I., Barr, A., Ciais, P., Davis, K., Dietze, M., Dragoni, D., Gough, C. M., Grant, R., Hollinger, D., Hufkens, K., Poulter, B., McCaughey, H., Raczka, B., Ryu, Y., Schaefer, K., Tian, H., Verbeeck, H., Zhao, M., and Richardson, A. D.: Terrestrial Bio-

sphere Model Performance for Inter-Annual Variability of Land-Atmosphere CO_2 Exchange, Global Change Biology, 18, 1971–1987, https://doi.org/10.1111/j.1365-2486.2012.02678.x, 2012.

380   Kolmogorov, A. N.: On Degeneration (Decay) of Isotropic Turbulence in an Incompressible Viscous Liquid, in: Dokl. Akad. Nauk SSSR, vol. 31, pp. 538–540, 1941.

Kolmogorov, A. N.: A Refinement of Previous Hypotheses Concerning the Local Structure of Turbulence in a Viscous Incompressible Fluid at High Reynolds Number, Journal of Fluid Mechanics, 13, 82–85, https://doi.org/10.1017/S0022112062000518, 1962.

Kwiatkowski, L., Torres, O., Aumont, O., and Orr, J. C.: Modified Future Diurnal Variability of the Global Surface Ocean CO_2 System,
385   Global change biology, 29, 982–997, https://doi.org/10.1111/gcb.16514, 2023.

Landschützer, P., Gruber, N., and Bakker, D. C. E.: Decadal Variations and Trends of the Global Ocean Carbon Sink, Global Biogeochemical Cycles, 30, 1396–1417, https://doi.org/10.1002/2015GB005359, 2016.

Liu, Z., Deng, Z., Davis, S. J., Giron, C., and Ciais, P.: Monitoring Global Carbon Emissions in 2021, Nature Reviews Earth & Environment, 3, 217–219, https://doi.org/10.1038/s43017-022-00285-w, 2022.

390   Obukhov, A. M.: The Structure of the Temperature Field in a Turbulent Flow, IZv. Akad. Nauk SSSR. Ser. Geogr. Geofia, 13, 1949.

Ohtaki, E.: On the Similarity in Atmospheric Fluctuations of Carbon Dioxide, Water Vapor and Temperature over Vegetated Fields, Boundary-Layer Meteorology, 32, 25–37, https://doi.org/10.1007/BF00120712, 1985.

Ohtaki, E., Tsukamoto, O., Iwatani, Y., and Mitsuta, Y.: Measurements of the Carbon Dioxide Flux over the Ocean, Journal of the Meteorological Society of Japan. Ser. II, 67, 541–554, https://doi.org/10.2151/jmsj1965.67.4_541, 1989.

395   Pathak, M., Slade, R., Shukla, P., Skea, J., Pichs-Madruga, R., and Ürge-Vorsatz, D.: Technical Summary, Climate Change 2022: Mitigation of Climate Change. Contribution of Working Group III to the Sixth Assessment Report of the Intergovernmental Panel on Climate Change, [P.R. Shukla, J. Skea, R. Slade, A. Al Khourdajie, R. van Diemen, D. McCollum, M. Pathak, S. Some, P. Vyas, R. Fradera, M. Belkacemi, A. Hasija, G. Lisboa, S. Luz, J. Malley, (eds.)], https://doi.org/10.1017/9781009157926.002, 2022.

Pritchard, D. T. and Currie, J. A.: Diffusion of Coefficients of Carbon Dioxide, Nitrous Oxide, Ethylene and Ethane in Air and Their
400   Measurement, Journal of Soil Science, 33, 175–184, https://doi.org/10.1111/j.1365-2389.1982.tb01757.x, 1982.

Richardson, L. F.: Weather Prediction by Numerical Process, Cambridge, The University press, 1922.

Roland, M., Serrano-Ortiz, P., Kowalski, A. S., Goddéris, Y., Sánchez-Cañete, E. P., Ciais, P., Domingo, F., Cuezva, S., Sanchez-Moral, S., Longdoz, B., Yakir, D., Van Grieken, R., Schott, J., Cardell, C., and Janssens, I. A.: Atmospheric Turbulence Triggers Pronounced Diel Pattern in Karst Carbonate Geochemistry, Biogeosciences, 10, 5009–5017, https://doi.org/10.5194/bg-10-5009-2013, 2013.

405   Sabine, C. L., Feely, R. A., Gruber, N., Key, R. M., Lee, K., Bullister, J. L., Wanninkhof, R., Wong, C. S., Wallace, D. W. R., Tilbrook, B., Millero, F. J., Peng, T.-H., Kozyr, A., Ono, T., and Rios, A. F.: The Oceanic Sink for Anthropogenic CO_2, Science, 305, 367–371, https://doi.org/10.1126/science.1097403, 2004.

Sahlée, E., Smedman, A.-S., Rutgersson, A., and Högström, U.: Spectra of CO_2 and Water Vapour in the Marine Atmospheric Surface Layer, Boundary-Layer Meteorology, 126, 279–295, https://doi.org/10.1007/s10546-007-9230-5, 2008.

410   Sarmiento, J. L. and Gruber, N.: Sinks for Anthropogenic Carbon, Physics Today, 55, 30–36, https://doi.org/10.1063/1.1510279, 2002.

Schmitt, F., Schertzer, D., Lovejoy, S., and Brunet, Y.: Empirical Study of Multifractal Phase Transitions in Atmospheric Turbulence, Nonlinear Processes in Geophysics, 1, 95–104, https://doi.org/10.5194/npg-1-95-1994, 1994.

Schmitt, F., Schertzer, D., Lovejoy, S., and Brunet, Y.: Multifractal Temperature and Flux of Temperature Variance in Fully Developed Turbulence, Europhysics Letters, 34, 195, https://doi.org/10.1209/epl/i1996-00438-4, 1996.

415 Schmitt, F. G.: Linking Eulerian and Lagrangian Structure Functions' Scaling Exponents in Turbulence, Physica A: Statistical Mechanics and its Applications, 368, 377–386, https://doi.org/10.1016/j.physa.2005.12.028, 2006.

Schmitt, F. G.: Gusts in Intermittent Wind Turbulence and the Dynamics of Their Recurrent Times, in: Wind Energy, edited by Peinke, J., Schaumann, P., and Barth, S., pp. 73–79, Springer Berlin Heidelberg, Berlin, Heidelberg, 2007.

Schmitt, F. G. and Huang, Y.: Stochastic Analysis of Scaling Time Series: From Turbulence Theory to Applications, Cambridge University
420 Press, 2016.

Schmitt, F. G., Dur, G., Souissi, S., and Brizard Zongo, S.: Statistical Properties of Turbidity, Oxygen and pH Fluctuations in the Seine River Estuary (France), Physica A: Statistical Mechanics and its Applications, 387, 6613–6623, https://doi.org/10.1016/j.physa.2008.08.026, 2008.

Seuront, L., Schmitt, F., Lagadeuc, Y., Schertzer, D., Lovejoy, S., and Frontier, S.: Multifractal Analysis of Phytoplankton Biomass and
425 Temperature in the Ocean, Geophysical Research Letters, 23, 3591–3594, https://doi.org/10.1029/96GL03473, 1996.

Sutton, A. J., Sabine, C. L., Maenner-Jones, S., Lawrence-Slavas, N., Meinig, C., Feely, R. A., Mathis, J. T., Musielewicz, S., Bott, R., McLain, P. D., Fought, H. J., and Kozyr, A.: A High-Frequency Atmospheric and Seawater pCO_2 Data Set from 14 Open-Ocean Sites Using a Moored Autonomous System, Earth System Science Data, 6, 353–366, https://doi.org/10.5194/essd-6-353-2014, 2014.

Sutton, A. J., Feely, R. A., Maenner Jones, S., Musielewicz, S., Osborne, J., Dietrich, C., Monacci, N. M., Cross, J. N., Bott, R., and Kozyr,
430 A.: Autonomous Seawater Partial Pressure of Carbon Dioxide (pCO_2) and pH Time Series from 40 Surface Buoys between 2004 and 2017 (NCEI Accession 0173932). NOAA National Centers for Environmental Information, https://doi.org/10.7289/V5DB8043, 2018.

Sutton, A. J., Feely, R. A., Maenner-Jones, S., Musielwicz, S., Osborne, J., Dietrich, C., Monacci, N., Cross, J., Bott, R., Kozyr, A., Andersson, A. J., Bates, N. R., Cai, W.-J., Cronin, M. F., De Carlo, E. H., Hales, B., Howden, S. D., Lee, C. M., Manzello, D. P., McPhaden, M. J., Meléndez, M., Mickett, J. B., Newton, J. A., Noakes, S. E., Noh, J. H., Olafsdottir, S. R., Salisbury, J. E., Send, U., Trull, T. W.,
435 Vandemark, D. C., and Weller, R. A.: Autonomous Seawater pCO_2 and pH Time Series from 40 Surface Buoys and the Emergence of Anthropogenic Trends, Earth System Science Data, 11, 421–439, https://doi.org/10.5194/essd-11-421-2019, 2019.

Thorpe, S. A.: The Turbulent Ocean, Cambridge University Press, Cambridge, 2005.

Thorpe, S. A.: An Introduction to Ocean Turbulence, Cambridge University Press, Cambridge, 2007.

Torres, O., Kwiatkowski, L., Sutton, A. J., Dorey, N., and Orr, J. C.: Characterizing Mean and Extreme Diurnal Variability of Ocean CO_2 Sys-
440 tem Variables Across Marine Environments, Geophysical Research Letters, 48, e2020GL090 228, https://doi.org/10.1029/2020GL090228, 2021.

Turk, D., Zappa, C. J., Meinen, C. S., Christian, J. R., Ho, D. T., Dickson, A. G., and McGillis, W. R.: Rain Impacts on CO_2 Exchange in the Western Equatorial Pacific Ocean, Geophysical Research Letters, 37, https://doi.org/10.1029/2010GL045520, 2010.

Wanninkhof, R.: Relationship between Wind Speed and Gas Exchange over the Ocean Revisited, Limnology and Oceanography: Methods,
445 12, 351–362, https://doi.org/10.4319/lom.2014.12.351, 2014.

Yamamoto, A., Abe-Ouchi, A., and Yamanaka, Y.: Long-Term Response of Oceanic Carbon Uptake to Global Warming via Physical and Biological Pumps, Biogeosciences, 15, 4163–4180, https://doi.org/10.5194/bg-15-4163-2018, 2018.

Yue, X.-L. and Gao, Q.-X.: Contributions of Natural Systems and Human Activity to Greenhouse Gas Emissions, Advances in Climate Change Research, 9, 243–252, https://doi.org/10.1016/j.accre.2018.12.003, 2018.

450 Zhang, M., Cheng, Y., Bao, Y., Zhao, C., Wang, G., Zhang, Y., Song, Z., Wu, Z., and Qiao, F.: Seasonal to Decadal Spatiotemporal Variations of the Global Ocean Carbon Sink, Global Change Biology, 28, 1786–1797, https://doi.org/10.1111/gcb.16031, 2022.

Zongo, S. B. and Schmitt, F. G.: Scaling Properties of pH Fluctuations in Coastal Waters of the English Channel: pH as a Turbulent Active

Scalar, Nonlinear Processes in Geophysics, 18, 829–839, https://doi.org/10.5194/npg-18-829-2011, 2011.